



Birefringence and transmission electron microscopy of monolayer and bilayer magnetoliposomes

P.C. Morais^{a,*}, K. Skeff Neto^{a,b}, P.P. Gravina^a, L.C. Figueiredo^a, M.F. Da Silva^a, Z.G.M. Lacava^c, R.B. Azevedo^c, L.P. Silva^c, M. De Cuyper^d

^aInstituto de Física, Núcleo de Física Aplicada, Universidade de Brasília, 70919-970 Brasília-DF, Brazil

^bFINATEC, 70910-900 Brasília-DF, Brazil

^cUniversidade de Brasília, Instituto de Ciências Biológicas, 70910-900 Brasília-DF, Brazil

^dInterdisciplinary Research Centre, Katholieke Universiteit Leuven, Campus Kortrijk, B-8500 Kortrijk, Belgium

Abstract

In this study, static magnetic birefringence (SMB) and transmission electron microscopy (TEM) were used to investigate magnetite-based monolayer and bilayer magnetoliposomes (MLs). The SMB data were analyzed using the recent model proposed by Skeff Neto et al. (J. Appl. Phys. 89 (2001) 3362). The SMB data indicate that monolayer-based MLs internalize magnetic nanoparticles as dimers while bilayer-based MLs internalize both isolated nanoparticles and dimers. The higher content of dimers inside monolayer MLs has been confirmed by TEM data.

© 2002 Elsevier Science B.V. All rights reserved.

Keywords: Birefringence; Domains; Magnetoliposome; Permeability; Transmission electron microscopy

The huge interest in producing biocompatible-coated solid material surfaces has lead, for instance, to the synthesis of magnetoliposomes (MLs) [1]. Briefly, MLs are physiologically stable structures consisting of a biocompatible vesicle filled with nanosized magnetic particles. Innovative applications of these structures deal with, for instance, oral drug-delivery systems [2] and magnetic resonance imaging markers for cancer diagnosis [3]. In this study, static magnetic birefringence (SMB) measurements, combined with transmission electron microscopy (TEM) data, is proposed as a promising strategy in the investigation of MLs.

Preparation of MLs used in this investigation starts with the synthesis of a laurate-coated magnetite-based magnetic fluid (MF) sample. In the second step the magnetite-coated MF sample was incubated with preformed phospholipid vesicles, while in the third step the resulting biocolloid was submitted

to a dialysis process. During this phase, the laurate molecules were changed for phospholipids. Depending on the amount of vesicles added, MLs surrounded by either a monolayer (ML1) or bilayer (ML2) are formed [4,5]. The actual concentration (C) of ML1 and ML2 was 4×10^{15} and 3×10^{15} particles/cm³, respectively. As a control, MF samples at the same concentration (4×10^{15} and 3×10^{15} particle/cm³) were also investigated. All SMB measurements were done at room temperature [6].

Figs. 1(a) and (b) show the SMB data of samples ML1 and ML2, respectively. Symbols represent experimental data while solid lines represent the best fit according to the model proposed in Ref. [7]. For comparison, MF1 and MF2 samples were also investigated and treated in the same way (not shown). The model used to fit the SMB data is an extension of the model proposed by Xu and Ridler [8] and deals with the field dependence of the magnetic permeability of chainlike magnetic structures (dimers for instance). In short, the SMB signal ($\Delta\bar{n}$) description includes the lognormal distribution function, $P(D)$ plus the magnetization associated to monomer and

*Corresponding author. Fax: +55-61-273655.

E-mail address: aderb@unb.br (P.C. Morais).

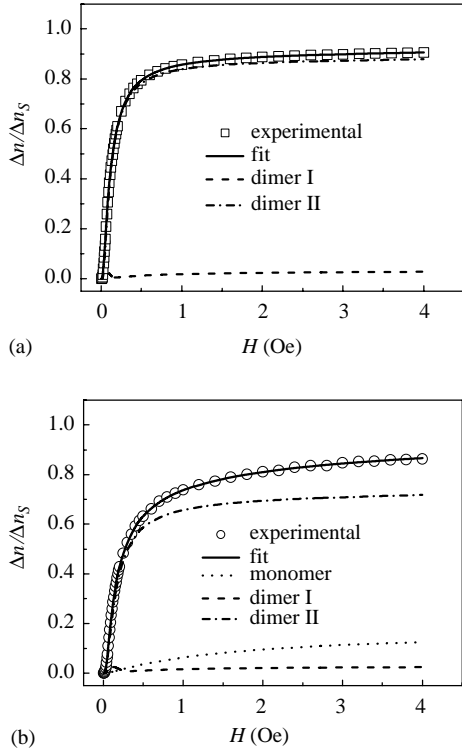


Fig. 1. Field dependence of the normalized SMB of (a) sample ML1 and (b) sample ML2. Symbols are experimental data while solid lines are the best fit using Eq. (1). Broken lines represent the contributions from monomers and dimers.

agglomerates:

$$\Delta\bar{n}(H; \bar{D}_B, \sigma_B, \bar{H}_Q, \sigma_Q) = A \frac{\int_0^\infty \left[\sum_Q C_Q \Delta n_Q(H, D) \right] D^3 P(D) dD}{\int_0^\infty D^3 P(D) dD} \quad (1)$$

with

$$\Delta n_Q(H, D) = \left[1 - \frac{3}{\xi_Q} \coth(\xi_Q) + \frac{3}{\xi_Q^2} \right].$$

The integral in Eq. (1) is carried out over $P(D)$, defined through the mean particle diameter (\bar{D}_B) and the standard deviation (σ_B), while the summation takes into account the particle agglomeration with C_Q (fraction of magnetic structure Q) constrained by $\sum_{Q=1}^Q C_Q = 1$. Note that the influence of chainlike structures (dimers and trimers for instance) in the low-field side of $\Delta\bar{n}$ versus H curve is to make it steeper.

The SMB data shown in Figs. 1(a) and (b) were best fitted assuming the presence of *monomers* (MM) and *dimers* (DM). $\xi_{MM} = (\pi/6)M_s D^3 H/kT$ accounts for monomer ($Q = 1$), while $\xi_{DM} = Q\xi_{MM}[1 +$

$\beta C_{DM} F_{DM}(H)]$ describes the dimer contribution ($Q = 2$), where M_s , k , T , and β are the magnetite saturation magnetization, the Boltzmann constant, and a constant, respectively. Notice that $[1 + \beta C_Q F_Q(H; \bar{H}_Q, \sigma_Q)]$ is a function related to the rotational magnetic permeability (μ_Q^r), where $F_Q(H; \bar{H}_Q, \sigma_Q)$ is the lognormal distribution function defined by the mean field (\bar{H}_Q) and by the standard deviation (σ_Q) [9]. At this point we should mention that a rotational permeability (μ_Q^r) as well as a rotational susceptibility (χ_Q^r) may be associated to a linear chain of monodomain magnetic nanoparticles consisting of Q single units, as discussed in more detail in Ref. [7].

Figs. 2(a) and (b) show the particle size histograms obtained from samples ML1 and ML2, respectively. The data (vertical bars) were obtained using TEM micrographs and curve fitted (solid lines) using the lognormal function

$$P(D) = \frac{\exp(-2\sigma_T^2)}{\bar{D}_T \sigma_T \sqrt{2\pi}} \exp\{-\ln^2(D/\bar{D}_T)/2\sigma_T^2\}$$

[10], with a mean particle diameter, \bar{D}_T , of 12.1 and 7.6 nm for ML1 and ML2, respectively. Standard

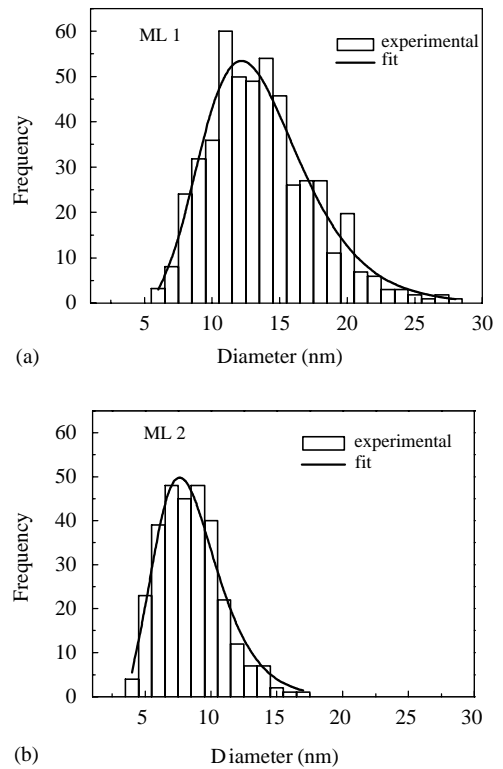


Fig. 2. Particle size histograms obtained from the TEM data from (a) sample ML1 and (b) sample ML2. Solid lines represent the best fit of the data according to Eq. (1).

Table 1

Some of the most relevant parameters obtained from the fit of the SMB data according to the model described by Eq. (1)

	ML1	ML2	MF1	MF2
C ($\times 10^{15} \text{ cm}^{-3}$)	4	3	4	3
\bar{D}_B (nm)	5.3	6.1	5.1	5.3
σ_B	0.32	0.28	0.34	0.32
C_1	—	0.17	0.08	0.29
C_2^I	0.03	0.03	0.03	0.02
C_2^{II}	0.97	0.80	0.89	0.69
\bar{H}_2^I (Oe)	56	88	80	82
\bar{H}_2^{II} (Oe)	398	321	499	505

deviations, σ_T , of 0.29 and 0.30 were obtained for ML1 and ML2, respectively. TEM analysis of the MF sample (not shown) allowed determination of the mean particle diameter (5.3 nm) and the standard deviation (0.32).

Four aspects related to Table 1 will be highlighted in what follows. First, except for sample ML2 the particle size polydispersity parameters obtained from the fitting of the SMB data are in excellent agreement with the parameters obtained from the TEM data. Second, sample ML1 presents only dimers inside the liposome units, while sample ML2 presents dimers (83%) plus monomers (17%). Third, dimer II (fanning) occurs at a much higher concentration as dimer I (coherent) [11]. Finally, the rotational permeability (μ_Q^r) associated to dimer II in both ML samples peak at lower field values as compared to the MF samples.

In summary, in this work, MLs are for the first time investigated using SMB measurements. Comparison of

the particle size profile obtained from SMB and TEM highlight the capability of birefringence measurements in assessing the mean size and size dispersion of magnetic structures inside MLs. In addition, a careful localization of the permeability peak would be extremely important in the design of hyperthermia systems, once heat-generation could be enhanced for field modulation around permeability peaks.

Financial support for this study was provided by the Brazilian agencies FAP-DF, CNPq, FINATEC, and CAPES and the Flemish *Fonds voor Wetenschappelijk Onderzoek*.

References

- [1] M. De Cuyper, M. Joniau, *Eur. Biophys. J.* 15 (1988) 311.
- [2] H. Chen, R. Langer, *Pharmacol. Res.* 14 (1997) 537.
- [3] S. Päufer, R. Reszka, S. Wagner, K.-J. Wolf, H.-J. Buhr, G. Berger, *Anti-Cancer Drug Des.* 12 (1997) 125.
- [4] G.W. Reimers, S.E. Khalafalla, US patent 3843540, 1974.
- [5] M. De Cuyper, M. Joniau, *Langmuir* 7 (1991) 647.
- [6] B.M. Lacava, R.B. Azevedo, L.P. Silva, Z.G.M. Lacava, K. Skeff Neto, N. Buske, A.F. Bakuzis, P.C. Morais, *Appl. Phys. Lett.* 77 (2000) 1876.
- [7] K. Skeff Neto, A.F. Bakuzis, P.C. Morais, A.R. Pereira, R.B. Azevedo, L.M. Lacava, Z.G.M. Lacava, *J. Appl. Phys.* 89 (2001) 3362.
- [8] M. Xu, P.J. Ridler, *J. Appl. Phys.* 82 (1997) 326.
- [9] C. Papusoi Jr., *J. Magn. Magn. Mater.* 195 (1999) 708.
- [10] B. Payet, D. Vincent, L. Delaunay, G. Noyel, *J. Magn. Magn. Mater.* 186 (1998) 168.
- [11] A.F. Bakuzis, M.F. Da Silva, P.C. Morais, L.S.F. Olavo, K. Skeff Neto, *J. Appl. Phys.* 87 (2000) 2497.